Identification of the tyrosine phosphatase PTP-MEG2 as an antagonist of hepatic insulin signaling

Charles Y. Cho,[1,2,6] Seung-Hoi Koo,[3,4,6] Yan Wang,[1] Scott Callaway,[5] Susan Hedrick,[3] Puiying A. Mak,[1] Anthony P. Orth,[1] Eric C. Peters,[1] Enrique Saez,[1] Marc Montminy,[3] Peter G. Schultz,[1,2,*] and Sumit K. Chanda[1,*]

[1] Genomics Institute of the Novartis Research Foundation, 10675 John Jay Hopkins Drive, San Diego, California 92121
[2] Department of Chemistry and The Skaggs Institute for Chemical Biology, The Scripps Research Institute, 10550 North Torrey Pines Road, La Jolla, California 92037
[3] Salk Institute for Biological Studies, 10010 North Torrey Pines Road, La Jolla, California 92037
[4] Department of Molecular Cell Biology, Sungkyunkwan University School of Medicine, Suwon 440-746, Korea
[5] Vala Sciences, Inc., 11099 North Torrey Pines Road, Suite 255, La Jolla, California 92037
[6] These authors contributed equally to this work.
*Correspondence: schultz@scripps.edu (P.G.S.); schanda@gnf.org (S.K.C.)

Summary

Insulin resistance is a primary defect in type 2 diabetes characterized by impaired peripheral glucose uptake and insufficient suppression of hepatic glucose output. Insulin signaling inhibits liver glucose production by inducing nuclear exclusion of the gluconeogenic transcription factor FOXO1 in an Akt-dependent manner. Through the concomitant application of genome-scale functional screening and quantitative image analysis, we have identified PTP-MEG2 as a modulator of insulin-dependent FOXO1 subcellular localization. Ectopic expression of PTP-MEG2 in cells inhibited insulin-induced phosphorylation of the insulin receptor, while RNAi-mediated reduction of PTP-MEG2 transcript levels enhanced insulin action. Additionally, adenoviral-mediated depletion of PTP-MEG2 in livers of diabetic (*db*/*db*) mice resulted in insulin sensitization and normalization of hyperglycemia. These data implicate PTP-MEG2 as a mediator of blood glucose homeostasis through antagonism of insulin signaling, and suggest that modulation of PTP-MEG2 activity may be an effective strategy in the treatment of type 2 diabetes.

Introduction

In the fasted state, glucose is synthesized by the liver to maintain euglycemia (Barthel and Schmoll, 2003). When blood glucose levels are elevated after nutrient ingestion, endogenous glucose production is downregulated. This response is primarily coordinated by insulin, which suppresses hepatic gluconeogenesis by reducing the expression of the key gluconeogenic enzymes phosphoenolpyruvate carboxykinase (PEPCK) and glucose-6-phosphatase (G6Pase). Liver insulin resistance, a major factor in the development of type 2 diabetes, leads to excessive postprandial glucose production and abnormal blood glucose levels.

Binding of insulin to its cognate receptor stimulates receptor tyrosine kinase activity, resulting in the phosphorylation of several substrates, including insulin receptor substrate (IRS) proteins (White, 2003). IRS phosphorylation leads to the recruitment and activation of type 1A phosphatidylinositol (PtdIns) 3-kinase, which catalyzes the formation of the lipid second messenger PtdIns(3,4,5)-trisphosphate [PtdIns(3,4,5)P_3] at the plasma membrane. Elevation of PtdIns(3,4,5)P_3 levels alters the localization and induces the activation of several protein kinases, including those of the Akt family (also known as protein kinase B). Loss of Akt2 function in mice results in insulin resistance and impaired glucose tolerance due to dysregulated hepatic glucose production and decreased uptake in skeletal muscle (Cho et al., 2001), demonstrating its critical role in insulin signaling.

Akt modulates G6Pase and PEPCK expression by suppressing the activity of FOXO1, a member of the forkhead family of transcription factors (reviewed in Accili and Arden, 2004 and Barthel et al., 2005). In the absence of insulin stimulation, FOXO1 is localized to the nucleus and acts in concert with the peroxisome proliferator-activated receptor-γ coactivator 1 α (PGC-1α) to increase gluconeogenic gene transcription (Puigserver et al., 2003). Upon insulin stimulation, Akt phosphorylates FOXO1 at three sites, inducing FOXO1 translocation to the cytoplasm and thereby reducing its transcriptional activity. Targeted expression of a constitutively nuclear FOXO1 mutant to the liver promotes diabetes in transgenic mice (Nakae et al., 2002). In contrast, FOXO1 haploinsufficiency restores insulin sensitivity in mice with defective insulin signaling (Nakae et al., 2002). Moreover, hepatic expression of a FOXO1 dominant-negative mutant reduces G6Pase and PEPCK expression and hepatic glucose output (Altomonte et al., 2003). FOXO1 has also been shown to mediate insulin-regulated hepatic expression of apolipoprotein CIII, a regulator of plasma triglyceride metabolism (Altomonte et al., 2004). These and other studies demonstrate that FOXO1 serves as a molecular link between insulin and changes in hepatic gene expression that, when dysregulated, can give rise to features of type 2 diabetes, including excessive hepatic glucose output and systemic hypertriglyceridemia.

Here, we have combined a genomics-based functional screening strategy with quantitative image analysis (also referred to as high content screening, image cytometry, or machine vision analysis) to identify novel modulators of FOXO1 subcellular localization. One such factor is the nonreceptor *p*rotein *t*yrosine *p*hosphatase (PTP)-MEG2 (or PTPN9), which when overexpressed, results in the nuclear accumulation of FOXO1. Forced expression of PTP-MEG2 in cell lines and in mouse liver

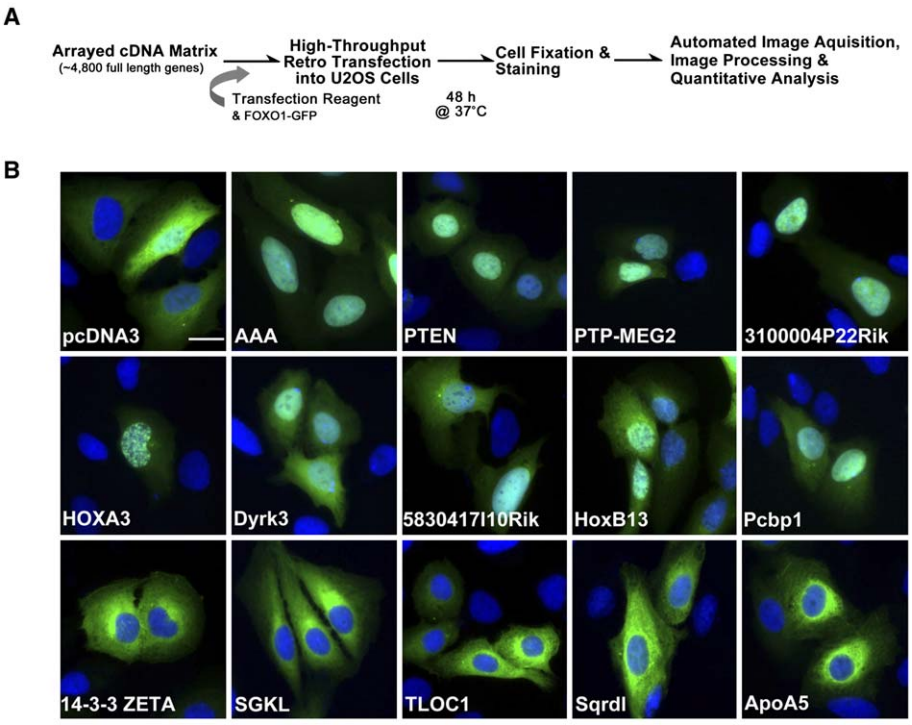

Figure 1. Screen for modulators of FOXO1 subcellular localization

A) Approximately 4800 human and mouse genes were individually cotransfected with a GFP-FOXO1 reporter. Plates were imaged using high-throughput fluorescence microscopy and the average percentage of GFP-FOXO1 localized in the nucleus was determined for each gene.

B) Cotransfection of GFP-FOXO1 with selected cDNAs identified through the genome-scale screen into U2OS cells. Nuclei are stained with DAPI (blue) while GFP-FOXO1 is shown in green. Cotransfection with empty vector pcDNA3 served as a negative control and constitutively nuclear FOXO1-GFP (AAA) is also shown. Ectopic expression of cDNAs increased FOXO1 nuclear localization more than 3.5 standard deviations from a calculated mean (row 1, column 3 through row 2, column 5), or resulted in further cytoplasmic accumulation of the transcription factor (>2 standard deviations; row 3, columns 1–5). The scale bar represents 20 μm.

decreases insulin receptor phosphorylation, while the reduction of PTP-MEG2 levels increases insulin-mediated suppression of FOXO1 activity in hepatoma cell lines and dramatically improves glucose tolerance in diabetic (*db/db*) mice. These results indicate a novel role for PTP-MEG2 in the negative regulation of hepatic insulin signaling.

Results

Image-based screen for FOXO1 regulators

To identify novel regulators of FOXO1 subcellular localization, arrayed full-length cDNAs from the Mammalian Genome Collection (Strausberg et al., 1999) were individually cotransfected with a GFP-FOXO1 reporter construct into U2OS osteosarcoma cells using a high-throughput methodology (Figure 1A; Chanda et al., 2003). After a 2 day incubation period, cells were fixed and stained with the DNA binding dye DAPI. Two sets of images (one each for the DAPI and GFP fluorophores) were collected using automated fluorescence microscopy and analyzed using CytoShop software (Beckman Coulter) (Harada et al., 2005). Image segmentation was initially performed upon images obtained from the DAPI channel. To ensure that only single cells were considered, all objects within the images which did not conform to experimentally determined parameters reflecting appropriate nuclear intensity and nuclear shape were excluded. The cytoplasm for each cell was then defined as an annulus of 30 pixels from the nuclear edge. Imaged GFP-expressing cells were then associated with their respective nuclei, and the percentage of FOXO1 localized in the nucleus (FLIN) was determined for each transfected cell and averaged for each well. Cells that had extreme FLIN values (>95% or <5%) were excluded from the analysis, since such measurements typically arose from segmentation or other artifacts (for example, GFP from the cytoplasm of a neighboring cell intersecting a nontransfected cell). To determine the effects of each encoded protein upon FOXO1 subcellular localization, the FLIN values of the middle 90% of transfected wells were averaged for each plate and used to define a plate mean and standard deviation. Subsequently, well activities were defined in terms of standard deviations from the plate mean (σ level).

In U2OS cells maintained under 10% serum conditions, GFP-FOXO1 is primarily localized in the cytoplasm but can also be found in both the cytoplasm and the nucleus in a fraction of the transfected population (Nakamura et al., 2000, Figure 1B). GFP-FOXO1 distribution is correlated with its expression levels, and this heterogeneity results in a median FLIN calculation of 50% in unperturbed cells. For comparison, transfection of a mutant GFP-FOXO1 construct, in which the three Akt phosphorylation sites are altered to alanine (T24A/S256A/S319A, referred to as AAA), results in nearly all of the GFP fluorescence colocalizing with the nucleus (FLIN value of 75%, 11 σ, Figure 1B). Cotransfection of GFP-FOXO1 with the lipid phosphatase PTEN, a known antagonist of PI3K/Akt signaling, results in dephosphorylation of the Akt-responsive residues in FOXO1 and a significant increase in the percentage of GFP-FOXO1 in the nucleus (FLIN 64%, 6σ, Figure 1B; Nakamura et al., 2000). In contrast, overexpression of Akt1 results in GFP-FOXO1 cytoplasmic localization (FLIN 40%, −2.5 σ, data not shown).

Ectopic expression of 14 genes identified through the screen was confirmed to induce FOXO1 nuclear localization by >3.5 σ, while ten encoded proteins promoted a decrease in levels of nuclear FOXO1 by >2 σ under these experimental conditions (Tables 1 and S1 in the Supplemental Data available with this article online). Several genes identified in the screen are known to be associated with the PI3K/Akt signaling pathway. The p85β subunit of PI3 kinase can act as a negative regulator of insulin signaling (Ueki et al., 2002), and its overexpression resulted in the strongest induction of GFP-FOXO1 nuclear localization (10 σ).

Table 1. Regulators of FOXO1 subcellular localization identified through genome-scale functional analysis

Accession	Gene Symbol	Name	Sigma level of nuclear FOXO1	Selected GO Annotations	Selected Interpro Domains
BC006796	Pik3r2*	phosphatidylinositol 3-kinase, regulatory subunit, polypeptide 2 (p85 beta)	9.61	insulin receptor signaling pathway (GO:0008286) phosphatidylinositol 3-kinase activity (GO:0016303)	PI3 kinase, P85 regulatory subunit (IPR001720)
BC010863	PTPN9/ PTP-MEG2	protein tyrosine phosphatase, nonreceptor type 9	9.01	protein tyrosine phosphatase activity (GO:0004725)	Phosphatidylinositol transfer protein-like, N-terminal (IPR011074);Protein tyrosine phosphatase, catalytic region (IPR003595)
BC011286	3100004P22Rik	hypothetical protein LOC68035	6.26	nuclear mRNA splicing, via spliceosome (GO:0000398)	RNA-binding region RNP-1 (RNA recognition motif) (IPR000504)
BC018480	Guca1b	guanylate cyclase activator 1B	6.19	Calcium sensitive guanylate cyclase activator activity (GO:0008048)	Calcium-binding EF-hand (IPR002048)
BC015180	HOXA3	homeo box A3	6.03	development (GO:0007275); regulation of transcription, DNA-dependent (GO:0006355)	Homeobox (IPR001356)
BC005821	PTEN*	phosphatase and tensin homolog (mutated in multiple advanced cancers 1)	6.00	phosphatidylinositol-3,4,5-trisphosphate 3-phosphatase activity (GO:0016314)	Protein tyrosine phosphatase, catalytic region (IPR003595)
BC010315	Tdg	thymine DNA glycosylase	5.91	hydrolase activity (GO:0016787)	Uracil-DNA glycosylase superfamily (IPR005122)
BC006704	Dyrk3	dual-specificity tyrosine-(Y)-phosphorylation-regulated kinase 3	4.94	protein serine/threonine kinase activity (GO:0004674)	Serine/threonine protein kinase (IPR002290)
BC011211	Mat1a	methionine adenosyltransferase I, alpha	4.91	ATP binding (GO:0005524)	S-adenosylmethionine synthetase (IPR002133)
BC016616	5830417I10Rik	hypothetical protein LOC76022	4.47		
BC013639	Hoxb13	homeo box B13	4.37	regulation of transcription, DNA-dependent (GO:0006355)	Homeobox (IPR001356)
BC004793	Pcbp1	poly(rC) binding protein 1	4.04	DNA binding (GO:0003677)	KH (IPR004087)
BC008602	PSTPIP1	proline-serine-threonine phosphatase interacting protein 1	3.79	endocytosis (GO:0006897)	Cdc15/Fes/CIP4 (IPR001060)
BC016509	SCAMP4	secretory carrier membrane protein	3.61	hydrolase activity (GO:0016787)	Cytidine/deoxycytidylate deaminase, zinc-binding region (IPR002125)
N/A	pSG5L	Control	0		
BC001263	SGK*	serum/glucocorticoid-regulated kinase	−2.05	protein serine/threonine kinase activity (GO:0004674)	Protein kinase (IPR000719)
BC011198	Apoa5	apolipoprotein A-V	−2.48	lipid transport (GO:0006869)	Apolipoprotein A/E/C3 (IPR009074)
BC000995	SFN*	stratifin (14-3-3 sigma)	−2.55	protein kinase C inhibitor activity (GO:0008426)	14-3-3 protein (IPR000308)
BC012035	TLOC1	translocation protein 1	−2.98	receptor activity (GO:0004872)	Translocation protein Sec62 (IPR004728)
BC010735	EEF1A1	eukaryotic translation elongation factor 1 alpha 1	−3.03	GTPase activity (GO:0003924); protein biosynthesis (GO:0006412)	EF-Tu/eEF-1alpha/eIF2-gamma, C-terminal (IPR009001)
BC016618	LCP2	lymphocyte cytosolic protein 2	−3.20	transmembrane receptor protein tyrosine kinase signaling pathway (GO:0007169)	Sterile alpha motif SAM (IPR001660)
BC011153	Sqrdl	sulfide quinone reductase-like (yeast)	−3.36	oxidoreductase activity (GO:0016491)	FAD-dependent pyridine nucleotide-disulphide oxidoreductase (IPR001327)
BC015326	SGKL*	serum/glucocorticoid-regulated kinase-like	−3.52	protein amino acid phosphorylation (GO:0006468)	Protein kinase (IPR000719)
BC003623	YWHAZ*	tyrosine 3-monooxygenase/ tryptophan 5-monooxygenase activation protein (14-3-3 zeta)	−3.89	protein domain specific binding (GO:0019904)	14-3-3 protein (IPR000308)
BC020963	YWHAG*	3-monooxygenase/tryptophan 5-monooxygenase activation protein, gamma polypeptide (14-3-3 gamma)	−4.13	insulin-like growth factor receptor binding (GO:0005159); negative regulation of protein kinase activity (GO:0006469)	14-3-3 protein (IPR000308)

High-throughput functional analysis revealed that overexpression of these cDNA clones lead to an increase (sigma level > 0) or decrease (sigma level < 0) in the fraction of GFP-FOXO1 localized to the nucleus, as compared to a negative control (pSG5L). Sigma levels are provided as a function of standard deviations to the mean score of nonresponders on a plate (see Experimental Procedures). All activities were subsequently reconfirmed in secondary assays. Selected GO annotations and InterPro domains for each encoded protein are also provided, and previously known or inferred regulators of FOXO1 are indicated with an asterisk (*).

Conversely, transfection of cDNAs encoding three 14-3-3 proteins (sigma, gamma, and zeta subtypes) increased GFP-FOXO1 cytoplasmic localization, possibly through direct binding to phosphorylated FOXO1 (Figure 1B; Brunet et al., 1999). Expression of the kinase serum/glucocorticoid-regulated kinase (SGK) also directed FOXO1 to the cytoplasm, an activity previously shown to be mediated by phosphorylation of FOXO1 at residues T24 and S319 (Brunet et al., 2001). The kinase SGKL,

which is highly homologous to SGK, also increases FOXO1 cytoplasmic localization. To our knowledge, the remaining 17 genes (Table 1) that affect FOXO1 nuclear localization have not previously been associated with PI3K/Akt signaling.

PTP-MEG2 reduces Akt-mediated FOXO1 phosphorylation

To test if the identified proteins regulate FOXO1 cellular distribution through modulation of the PI3K/Akt pathway, cDNAs whose overexpression resulted in increased nuclear localization of the transcription factor were cotransfected with FOXO1 in U2OS cells. Western blot analysis revealed that transfection of several genes, including PTP-MEG2/PTPN9, reduced phosphorylation levels of FOXO1 at S256, a residue which is targeted by Akt kinase activity (Figures 2A and S1A, data not shown). Consistent with the observed inhibition of Akt activity, phosphorylation of endogenous Akt at S473, a PDK2 phosphorylation site, was also reduced subsequent to transfection of PTP-MEG2 (Figure 2A), suggesting that expression of PTP-MEG2 reduces PtdIns(3,4,5)P_3 concentration at the plasma membrane.

PTP-MEG2 was one of the most potent regulators of FOXO1 localization identified through the large-scale screen (Table 1); therefore this phosphatase was chosen for further study. To confirm that the observed role of PTP-MEG2 was not due to nonspecific activities associated with the overexpression of a phosphatase, we monitored FOXO1 subcellular localization after cotransfection with two other PTPs. The ectopic expression of PTP-MEG1 and TC-PTP (transcript variant 2) resulted in a marginal increase of GFP-FOXO1 in the nucleus (2.1% and 7%, respectively), whereas the introduction of PTP-MEG2 resulted in a 62% increase in FOXO1 nuclear localization (Table S1). We next constructed mutants of PTP-MEG2 which disrupted either the phosphatase or conserved Sec14p homology domains in the protein. We ectopically expressed wild-type PTP-MEG2 and these mutants in U2OS cells and quantitated the effect on FOXO1 localization. While PTP-MEG2 overexpression resulted in a 71% FLIN value, the effect of the catalytically inactive PTP-MEG2 (C515S) mutant was comparable to activities observed with negative controls (54% FLIN, Figure 2B). In addition, expression of a truncated PTP-MEG2, containing only the catalytic domain, did not result in a significant increase in FOXO1 translocation (57% FLIN; Figure 2B). These results indicate that both phosphatase activity and the Sec14p homology domain are required for PTP-MEG2 to potentiate FOXO1 nuclear localization.

PTP-MEG2 has been previously reported to promote secretory vesicle fusion (Wang et al., 2002, 2005; Huynh et al., 2003). To investigate whether the observed effects of PTP-MEG2 on FOXO1 subcellular localization could be due to its ability to regulate cellular secretion processes, we cotransfected a plasmid encoding secreted alkaline phosphatase (SEAP) along with plasmids encoding wild-type or catalytically inactive PTP-MEG2 into U2OS cells. Expression of neither protein resulted in a reduction of SEAP concentrations in the culture media, indicating that the effects of PTP-MEG2 upon FOXO1 signaling are likely independent of global effects upon secretory pathways (Figure S1B).

Ectopic expression of PTP-MEG2 antagonizes insulin signaling

To determine if ectopic expression of the tyrosine phosphatase PTP-MEG2 would affect the transcription of hepatic insulin-responsive genes, PTP-MEG2 was cotransfected with a construct containing G6Pase enhancer elements upstream of a luciferase reporter gene into HepG2 cells. Wild-type PTP-MEG2 expression attenuated insulin-mediated repression of G6Pase expression (Figure 2C), while the catalytically inactive PTP-MEG2 (C515S) did not. Insulin treatment had no effect on the activity of a mutant G6Pase reporter construct that is unresponsive to FOXO1; the activity of the mutant construct was also unperturbed by the expression of PTP-MEG2. Moreover, adenoviral-mediated PTP-MEG2 overexpression in primary rat hepatocytes blocked insulin-stimulated repression of endogenous PEPCK expression as monitored by quantitative polymerase chain reaction (PCR) (Figure 2D), confirming the effect of PTP-MEG2 in a physiologically relevant context. Taken together, these data demonstrate that PTP-MEG2 activity opposes insulin-mediated repression of gluconeogenic gene transcription.

To explore the molecular basis of PTP-MEG2 activity responsible for this observed antagonism of insulin signaling, PTP-MEG2 was overexpressed in HEK-293A cells which were serum-starved and treated with insulin-like growth factor-1 (IGF-1). Immunoprecipitation-mass spectrometry analysis of PTP-MEG2-transfected and control lysates using an anti-phosphotyrosine antibody (Salomon et al., 2003) revealed decreased levels of IRS-1 and IGF-1 receptor tyrosine phosphorylation in cells receiving exogenous PTP-MEG2 (data not shown). To verify that PTP-MEG2 activity results in the dephosphorylation of insulin/IGF1 receptors, a vector control, PTP-MEG2, and PTP-MEG2 (C515S) were transiently transfected into HEK-293A followed by serum starvation and insulin treatment. Immunoprecipitation of the insulin receptor β subunit followed by immunoblotting and probing with the anti-phosphotyrosine antibody 4G10 confirmed that PTP-MEG2 overexpression reduces insulin-stimulated insulin receptor phosphorylation (Figure 2E). Immunoblots of lysates from PTP-MEG2-transfected cells reveal that PTP-MEG2 expression reduces phosphorylation at Tyr1162/1163 (Figures 2F and S2A), which is required for its kinase activity (Ellis et al., 1986). Similar results were obtained when we assessed the effects of PTP-MEG2 expression upon IGF stimulation of insulin receptor autophosphorylation or IGF-mediated phosphorylation of the InsR substrate IRS1 (Figures S2B and S2C). These data implicate PTP-MEG2 as an antagonist of insulin receptor catalytic activity.

Reduction in PTP-MEG2 expression enhances insulin action

To assess whether endogenous PTP-MEG2 activity attenuates insulin receptor signaling, RNA interference was used to reduce PTP-MEG2 expression in the hepatocellular carcinoma HepG2 cell line. Transfection of a 21-mer duplex RNA oligonucleotide directed against human PTP-MEG2, as well as a mixture of four oligonucleotides (Smartpool), reduced PTP-MEG2 protein levels by approximately 55% and 40%, respectively (Figures 3A and S3). Decreased PTP-MEG2 levels resulted in enhancement of insulin receptor autophosphorylation in response to insulin (Figures 3A and S3). In addition, PTP-MEG2 inhibition also augmented the phosphorylation of Akt in response to insulin, consistent with an increase in levels of insulin signaling (Figure 3A). These results confirm that decreased PTP-MEG2 potentiates insulin signaling in insulin-responsive cell types.

Since reduction of PTP-MEG2 protein levels increases insulin-mediated insulin receptor phosphorylation, loss of PTP-MEG2

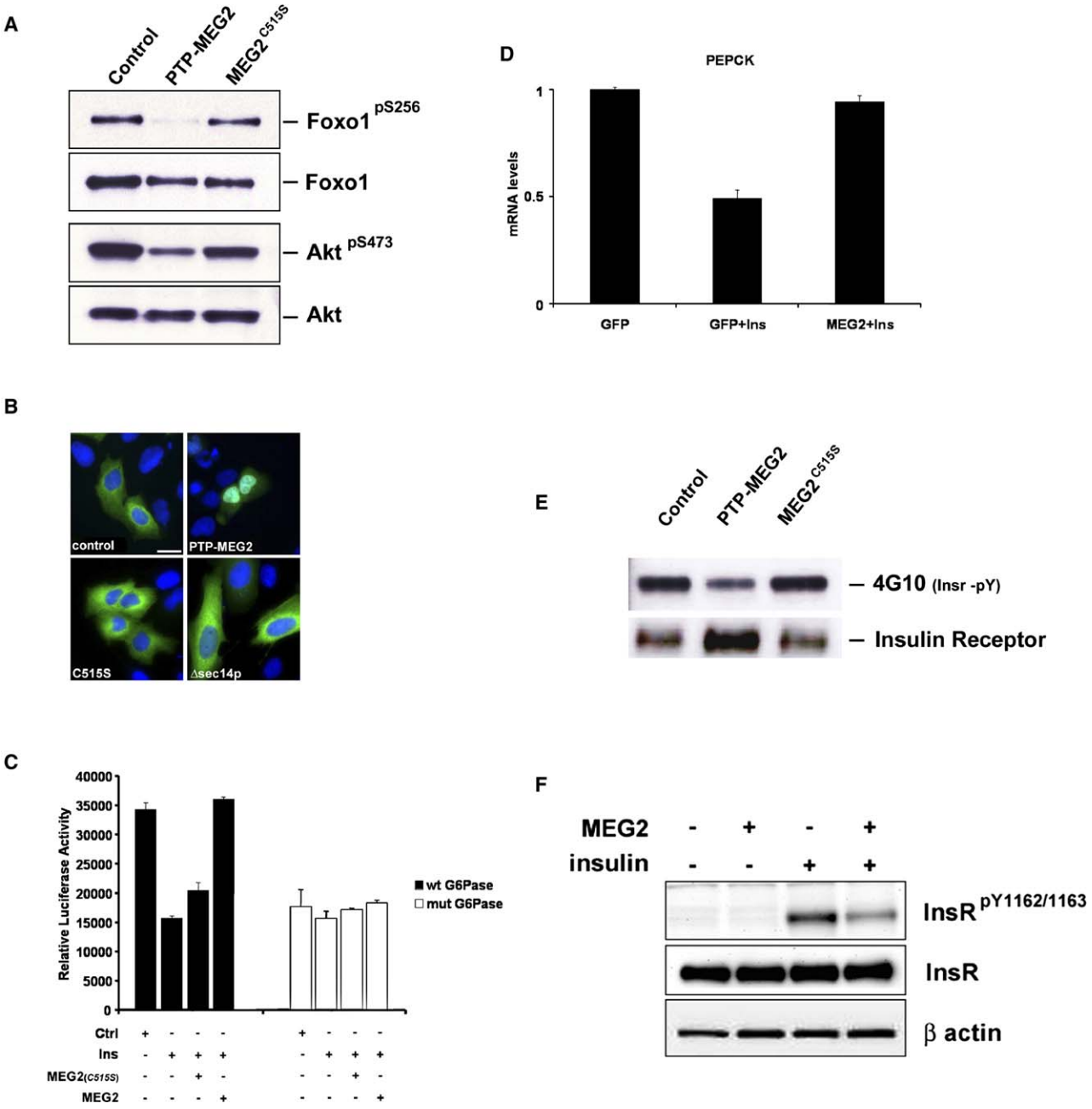

Figure 2. PTP-MEG2 modulates insulin signaling in cultured cells

A) HEK-293A cells were cotransfected with a vector control, PTP-MEG2, or catalytically inactive PTP-MEG2 (C515S) with GFP and FOXO1. After fluorescence-activated cell sorting, cells were grown in 10% FBS/DMEM and lysates were analyzed by immunoblot. PTP-MEG2 overexpression reduced both phosphorylation of FOXO1 at Ser256 (Akt phosphorylation site) and Akt at S473.

B) Catalytic activity and Sec14p homology domain are required for PTP-MEG2 induction of FOXO1 nuclear translocation. Control vector pcDNA3, PTP-MEG2, PTP-MEG2 (C515S), or PTP-MEG2 catalytic subunit (ΔSec14) were cotransfected with GFP-FOXO1. Images were acquired as in Figure 1. The scale bar represents 20 μm.

C) PTP-MEG2 overexpression alters the transcriptional response of a glucose-6-phosphatase reporter construct in HepG2 cells and is dependent on FOXO1 binding sites. Insulin treatment reduces the G6Pase luciferase reporter activity, but this effect is reversed by wild-type PTP-MEG2. The catalytically inactive PTP-MEG2 (C515S) mutant has no effect. A reporter construct in which the FOXO1 binding sites are mutated shows no response to either insulin treatment or PTP-MEG2 expression.

D) PTP-MEG2 blunts insulin-dependent inhibition of gluconeogenic gene expression. Quantitative PCR analysis of PEPCK transcripts was performed with RNA from rat primary hepatocytes infected with either GFP virus or PTP-MEG2 expression virus. For insulin treatment, cells were starved overnight, and 100 nM insulin was added for 8 hr.

E) PTP-MEG2 overexpression results in a decrease in insulin receptor tyrosine phosphorylation. HEK-293A cells were transfected with a vector control, PTP-MEG2, or PTP-MEG2 (C515S) and serum starved. Cells were treated with insulin (10 nM for 30 min) and then lysed. Insulin receptor was immunoprecipitated and immunoblots were probed with the anti-phosphotyrosine antibody 4G10.

F) PTP-MEG2 expression induces dephosphorylation of insulin receptor residues Y1162/Y1163. HEK-293A cells were transfected with PTP-MEG2 or a vector control, serum starved, and treated with insulin (20 nM for 30 min). Lysates were prepared and equal quantities of total protein were loaded on to an SDS-PAGE gel for immunoblot analysis with the anti-InsR pY1162/1163 antibody. Levels of insulin receptor and β-actin were measured as controls for loading. Error bars represent standard deviations from the experimental mean of at least three independent experiments.

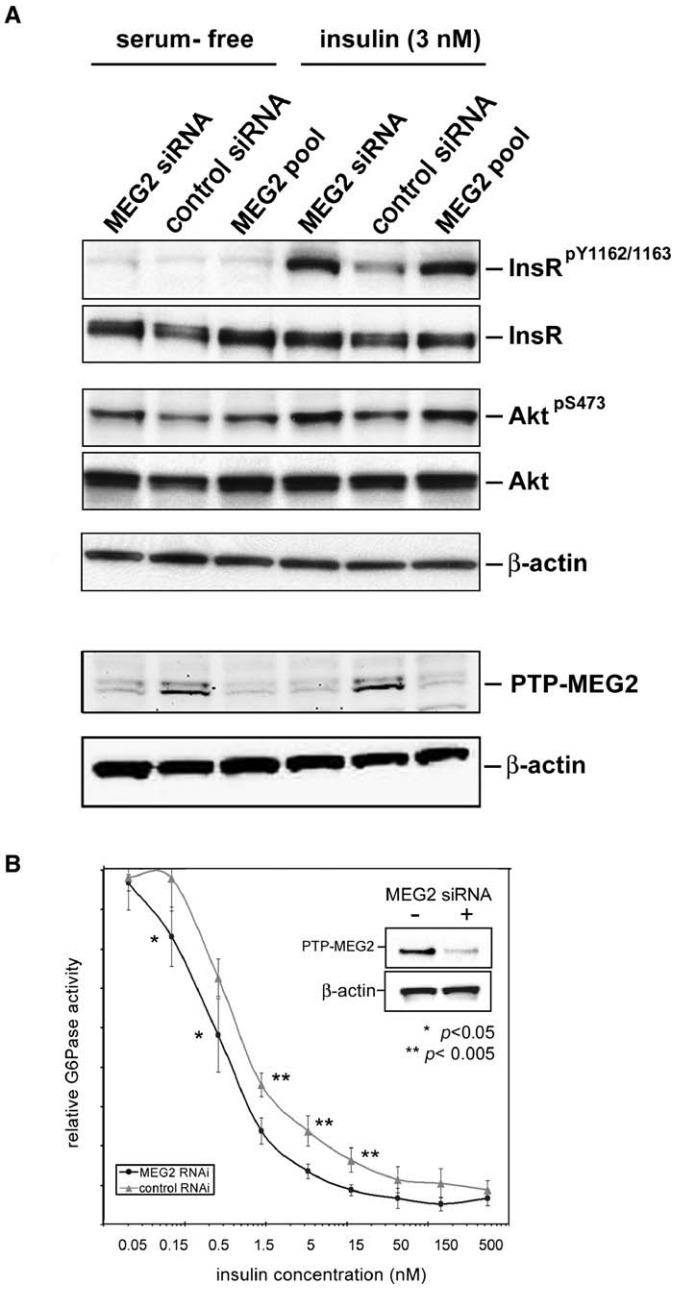

Figure 3. Reduction of PTP-MEG2 expression via RNA interference potentiates insulin activity in hepatoma cell lines

A) Human HepG2 cells were transfected with an RNA duplex targeting PTP-MEG2, an RNA duplex against a control (mouse Trb3) sequence that does not target any human genes, or a mixture of four RNA duplexes against PTP-MEG2 (Dharmacon Smartpool). After serum starvation and insulin treatment (3 nM for 30 min), lysates were prepared, and immunoblots were probed with the antibodies shown.

B) Reduction of PTP-MEG2 expression potentiates insulin repression of G6Pase expression in H4IIE cells. G6Pase-luc/H4IIE cells were infected with either PTP-MEG2 or control shRNA adenoviruses. Efficacy of RNAi treatment was measured by Western blot analysis with antibodies specific for PTP-MEG2 and β-actin (inset). Cells were serum starved and treated with dexamethasone (25 μM) and indicated concentrations of insulin. Activities for each replicate were normalized against PBS-treated cells.

p values were determined using two-sample assuming equal variances t test. Each data point represents the mean (±SD) of at least three independent experiments.

function would be expected to enhance insulin's suppression of gluconeogenic target genes in liver cell lines. To test this hypothesis, an adenovirus encoding a short hairpin RNA targeted against the rodent PTP-MEG2 sequence (Ad-MEG2 shRNA) was generated. H4IIE rat hepatoma cells, harboring an integrated luciferase reporter linked to G6Pase enhancer elements, were infected with the Ad-MEG2 shRNA. Infection with Ad-MEG2 shRNA resulted in a 50% reduction of PTP-MEG2 protein expression, as compared to control-infected cells (Figure 3B, inset). Decreased PTP-MEG2 expression resulted in approximately a 2-fold increase in insulin responsiveness (Control IC_{50} 1.05 nM, MEG2 RNAi IC_{50} 0.55 nM), as measured by the dose response of G6Pase-luc reporter activity (Figure 3B).

Increased PTP-MEG2 expression in liver suppresses insulin signaling

To test the activity of PTP-MEG2 on insulin action in vivo, we constructed adenoviruses that express PTP-MEG2 or GFP as a negative control. Following tail-vein injection into mice, the PTP-MEG2 adenovirus conferred increased expression of PTP-MEG2 in the liver (Figure 4A). No differences in basal blood glucose concentrations could be detected between the GFP and PTP-MEG2-infected mice (Figure S4A). To test their response to insulin, infected mice were injected with a bolus of either insulin or PBS after a 4 hr fast, and protein extracts from liver were examined by Western blot analysis. PTP-MEG2 overexpression decreased insulin receptor, GSK3-β, and Akt phosphorylation (Figures 4A, S4B, and S4C) after insulin stimulation. To assess the effect of PTP-MEG2 expression on glucose homeostasis, we conducted glucose tolerance tests (GTT) on PTP-MEG2 and GFP-expressing mice. During the GTT, PTP-MEG2-mice had consistently higher levels of blood glucose compared to GFP-injected mice, particularly at the 15 min ($p < 0.04$) and 30 min ($p < 0.02$) time points after glucose injection (Figure 4B). Furthermore, the behavior of blood glucose levels during insulin tolerance tests (ITT) indicated that forced hepatic PTP-MEG2 expression results in decreased insulin sensitivity (Figure 4C). These results demonstrate that elevated levels of PTP-MEG2 expression suppress insulin signaling in the liver and may contribute to insulin resistance.

PTP-MEG2 expression in the liver increases during fasting

We next investigated whether PTP-MEG2 expression levels in mouse liver were affected by fasting and refeeding conditions. Adult male C57Bl/6 mice (n = 6 per group) were fasted for 16 hr, or fasted for 24 hr and refed for another 24 hr. Total RNA was prepared from liver and PTP-MEG2 and phosphoenolpyruvate carboxykinase (PEPCK) expression levels were measured using quantitative RT-PCR (Figure 4D). As expected, PEPCK expression increased 141% during fasting ($p < 0.001$) and returned to normal after refeeding. PTP-MEG2 expression levels also increased in the livers of fasted mice (33%, $p < 0.001$), but were 21% lower in refed mice ($p < 0.001$) compared to fed mice. These data reveal that PTP-MEG2 expression is inversely related to insulin levels, suggesting that PTP-MEG2 is transcriptionally responsive to systemic alterations of insulin concentration.

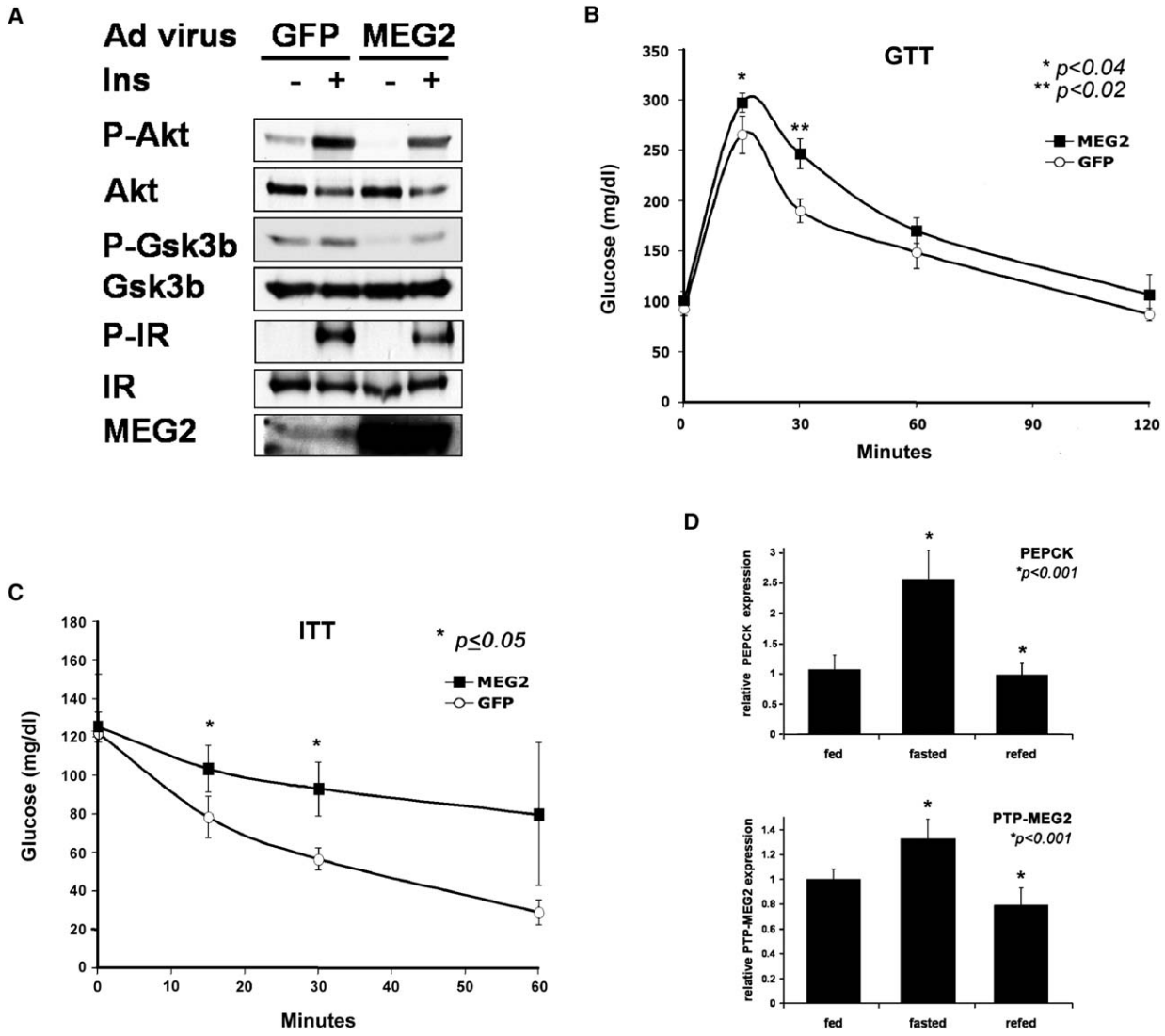

Figure 4. Transgenic PTP-MEG2 inhibits suppression of hepatic glucose output

A) PTP-MEG2 expression inhibits insulin signaling. Western blot analysis was performed with protein extracts from mouse liver infected with either GFP virus or MEG2 expression virus. Livers were collected after a bolus of insulin or PBS injection. Levels of PTP-MEG2 and total and phosphorylated forms Akt, Gsk3β and Insulin Receptor (IR) are shown.

B) PTP-MEG2 overexpression in mouse liver leads to impaired glucose tolerance. Mice injected with either GFP control virus or PTP-MEG2 expression virus were used for glucose tolerance test.

C) Ectopic expression of PTP-MEG2 induces insulin resistance. Mice infected with either control or PTP-MEG2 adenovirus were used for insulin tolerance test.

D) PTP-MEG2 expression is elevated under fasting conditions. Quantitative PCR analysis of PTP-MEG2 and PEPCK transcripts was done with RNA from livers of fed, fasted (16 hr), or refed adult male mice (n = 6). Relative PTP-MEG2 or PEPCK expression was normalized to that of 36B4 ribosomal protein RNA in each sample. PTP-MEG2 levels were significantly increased ($p < 0.001$) during fasting when compared to refed samples.

p values were calculated with the Student's t test and are indicated. Each point represents the mean (±SD) of at least three independent experiments.

Hepatic silencing of PTP-MEG2 improves insulin sensitivity in *db*/*db* mice

To ascertain whether modulation of PTP-MEG2 activity can restore insulin sensitivity and glycemic regulation in diabetic mice, we introduced adenovirus encoding a siRNA-hairpin directed against PTP-MEG2 to the liver of these animals. After fasting, mice were injected with insulin, and livers were harvested and analyzed by Western blot analysis. When compared to liver extracts from nonspecific RNAi-treated mice, hepatic reduction of PTP-MEG2 levels resulted in an increase in insulin signaling as assessed by the phosphorylation status of insulin receptor and Akt (Figure 5A, S5A, and S5B). Correspondingly, the insulin-stimulated transcriptional repression of the gluconeogenic genes PGC-1α and G6Pase was also markedly augmented in these animals (Figure 5B). We next performed glucose tolerance tests (GTT) on *db*/*db* mice injected with adenovirus encoding MEG2 or control siRNAs. These studies reveal that attenuation of hepatic PTP-MEG2 expression in *db*/*db* mice leads to in a significant reduction in both the amplitude and duration of elevated blood sugar levels (Figure 5C). Finally, we measured blood glucose levels in the MEG2 and control siRNA-infected *db*/*db* mice either under fasted conditions or an ad libitum feeding regimen. Reduction of PTP-MEG2 resulted in a decrease in blood glucose levels during fasting and lead to a significant reversal of

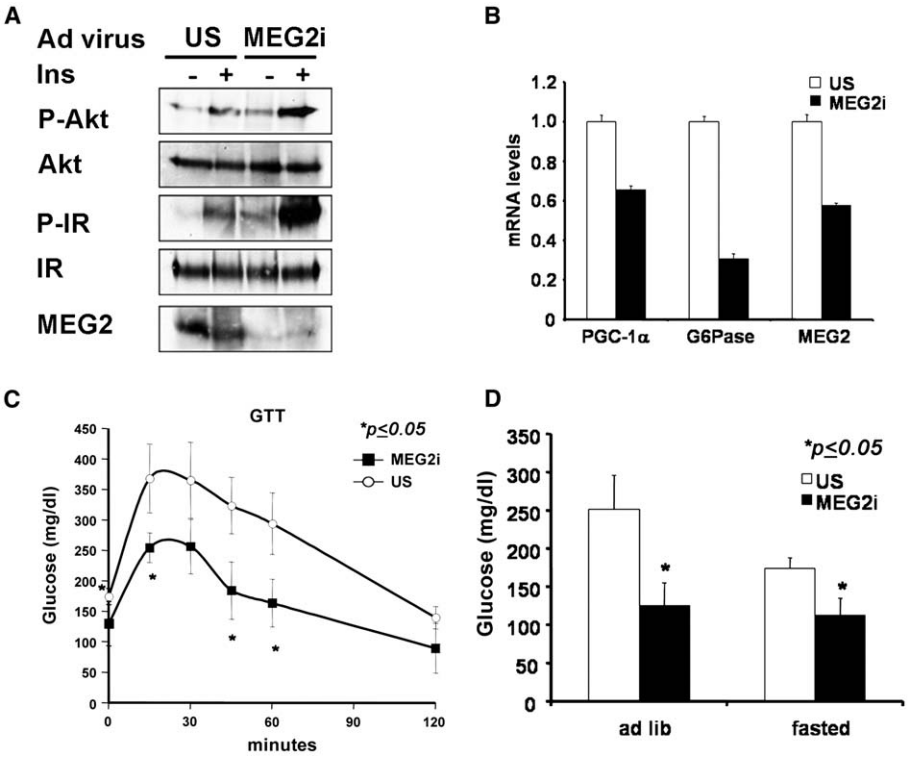

Figure 5. Reduction of hepatic PTP-MEG2 levels in diabetic mice results in insulin sensitization

A) Silencing of PTP-MEG2 in the liver of *db*/*db* mice leads to an increased response to insulin. Livers were collected from *db*/*db* mice infected with either an siRNA targeting PTP-MEG2 (MEG2i) or a control sequence (US) after bolus injection of insulin or PBS. Western blot analysis was performed with liver-derived protein extracts to determine levels of PTP-MEG and total and phosphorylated forms of Akt and Insulin receptor (IR).

B) Reduction of PTP-MEG2 levels potentiates insulin-induced repression of gluconeogenic target genes. RNA was collection from *db*/*db* mouse livers as described in (**A**), and quantitative RT-PCR was performed using primer and probe sets specific for PGC-1α, G6Pase, and PTP-MEG2. mRNA levels were normalized to an internal control, and values for the control siRNA-treated mice were set to 1.

C) Improved glucose clearance mediated by suppression of PTP-MEG2. Mice injected with either control virus (US) or PTP-MEG2 (MEG2i) siRNA virus were used for glucose tolerance test.

D) Hepatic silencing of PTP-MEG reverses hyperglycemia. Ad lib or 4 hr fasting blood glucose levels were measured in *db*/*db* mice injected with US/MEG2 RNAi adenovirus.

p values were calculated with the Student's t test and are indicated. Each point represents the mean (±SD) of at least three independent experiments.

hyperglycemia under ad lib feeding (Figure 5D). Taken together, these data indicate that the antagonism of PTP-MEG2 activity can restore insulin sensitivity and improve glycemic regulation in diabetic mice.

Discussion

We have profiled a library containing approximately 4800 full-length human and mouse cDNAs to identify novel regulators of the pleiotropic transcription factor FOXO1. The library was screened in an arrayed format, which allowed us to individually interrogate the activity of each encoded protein within the matrix. To monitor the cellular distribution of FOXO1, we employed an automated fluorescence microscopy platform in conjunction with pattern recognition and image analysis software. This enabled robust and accurate assessment of the fraction of FOXO1 localized to the nucleus (FLIN) in over 150,000 acquired images at the level of individually transfected cells. This represents a generally applicable methodology towards the genome-wide analyses of factors that regulate protein subcellular localization in response to extracellular stimuli.

The FOXO1 transcriptional program governs a number of distinct cellular processes, including oncogenesis, metabolic function, differentiation, and survival (Accili and Arden, 2004 and Barthel et al., 2005). In response to various extracellular stimuli, FOXO1 is phosphorylated by Akt and SGK and subsequently sequestered in the cytoplasm, thus abolishing forkhead target gene expression. In addition to Akt signaling, several other pathways can regulate FOXO activity. For example, cellular stress induces acetylation of FOXO proteins by p300/CBP-associated factor PCAF, while expression of the nutrient sensing HDAC Sirt1 results in FOXO deacetylation (Brunet et al., 2004; Motta et al., 2004). Although several genes identified in the screen have been previously implicated in the regulation of FOXO1, this functional assay also revealed seventeen novel mediators of FOXO1 subcellular localization in U2OS cells. Not surprisingly, these encoded proteins belong to a broad range of functional classes: kinases and other phosphorylation-related proteins, transcription factors, enzymes, trafficking proteins, lipid binding proteins, as well as proteins without assigned function. Since the genome-scale assay was executed under undefined growth factor conditions (10% serum), it is unclear if the proteins elucidated in the screen are influencing FOXO1 localization in U2OS cells through the modulation of signaling induced by insulin or other growth factors contained in the media. Further study will be required to characterize the functional role of gene products identified through this approach in the modulation of FOXO1 activity.

The screen revealed a previously unidentified role for the non-receptor protein tyrosine phosphatase PTP-MEG2 as potent inducer of FOXO1 nuclear localization. Interestingly, PTP-MEG2 has been previously implicated in the regulation of homotypic vesicle fusion in hematopoetic cell types (i.e., mast cells, T cells, and granulocytes; Wang et al., 2002). Furthermore, T lymphocytes derived from mice lacking PTP-MEG2 displayed defects in interleukin 2 secretion (Wang et al., 2005). The phosphatase regulates the secretory pathway through dephosphorylation of the fusion protein N-ethylmaleimide-sensitive factor (NSF; Huynh et al., 2004). However, we were not able to detect any effects of PTP-MEG2 overexpression upon global secretory mechanisms in U2OS (osteosarcoma) cells (Figure S1B). We speculate that the regulation of vesicle fusion events by PTP-MEG2 may be restricted to certain cell types, and the phosphatase possesses pleiotropic activities that are likely dependent on tissue-specific expression of its substrates, such as NSF (Su et al., 2004; http://symatlas.gnf.org). We further conclude

that the observed effects of PTP-MEG2 upon glucose homeostasis are likely due to direct modulation of insulin signaling and are exclusive of its previously described role in vesicle fusion. Since FOXO1 has an essential role in the control of liver glucose production, we further characterized PTP-MEG2 activity within the context of insulin signal transduction, although it is possible that the phosphatase may also act as a negative regulator of other growth factor pathways. Ectopic PTP-MEG2 expression blunts insulin-mediated transcriptional repression of gluconeogenic genes. Furthermore, overexpression of PTP-MEG2, both in vitro and in vivo, results in a coordinate reduction in phosphorylation levels of Akt, IRS-1, and the insulin receptor (InsR) proteins. These results suggest that PTP-MEG2 regulates insulin signal transduction by attenuating the activation of the insulin receptor but does not distinguish between a role for PTP-MEG2 regulating InsR activity through direct dephosphorylation of the receptor or by the modulation of a secondary, yet unidentified, protein. The immediate substrate of PTP-MEG2 phosphatase activity is currently under investigation. Conversely, reduction of PTP-MEG2 expression levels with RNAi-targeting sequences in hepatoma cell lines augments the cellular response to insulin, and silencing PTP-MEG2 in the livers of diabetic (*db*/*db*) mice resulted in a reversal of insulin resistance and hyperglycemia. These results indicate that PTP-MEG2 regulates glucose homeostasis and hepatic insulin action through the modulation of insulin receptor signaling.

Several PTPs have been previously implicated in the inhibition of insulin signal transduction, most notably PTP-1b (see Asante-Appiah and Kennedy, 2003 for a review). PTP-1b$^{-/-}$ mice have improved insulin sensitivity compared to wild-type controls and are resistant to weight gain when fed a high-fat diet (Elchebly et al., 1999; Klaman et al., 2000). PTP-1b is localized to the cytoplasmic surface of the endoplasmic reticulum, and dephosphorylates receptor tyrosine kinases after receptor endocytosis (Haj et al., 2002). The roles of other protein tyrosine phosphatases (PTPs) in insulin signaling are more complex. Overexpression of the transmembrane PTP leukocyte antigen-related phosphatase (LAR) in muscle results in whole-body insulin resistance (Zabolotny et al., 2001), and LAR-deficient mice have low insulin and glucose levels (Ren et al., 1998). However, LAR$^{-/-}$ mice are resistant to insulin-mediated suppression of hepatic glucose output (Ren et al., 1998). TCPTP, which is closely related to PTP-1b, has also been reported to have insulin receptor phosphatase activity (Galic et al., 2003). Interestingly, recent studies of insulin receptor activation in PTP-1b$^{-/-}$ and TCP-TP$^{-/-}$ mouse embryo fibroblasts suggest that even these closely related PTPs have nonoverlapping phosphatase activities since insulin receptor dephosphorylation occurs with distinct time courses (Galic et al., 2005).

PTPs are a diverse enzyme family with at least 107 members in the human genome (Alonso et al., 2004). Of these, only PTP-MEG2 possesses a 250 amino acid lipid binding domain that is homologous to Sec14p, a yeast protein with phosphatidylinositol (PtdIns) transferase activity. Our overexpression analysis indicates that the Sec14p homology domain is required for PTP-MEG2-mediated FOXO1 nuclear translocation in U2OS cells (Figure 2B). Biochemical and colocalization studies have indicated that the Sec14p domain in PTP-MEG2 binds to several phosphoinositides, including Ptd(3,5)P_2, Ptd(4,5)P_2, and Ptd(3,4,5)P_3 (Huynh et al., 2003; Kruger et al., 2002), or possibly to phosphatidylserine (Zhao et al., 2003). A number of phosphatidylinositol kinases and phosphatases are involved in various stages of insulin signaling and receptor tyrosine kinase processing, including p110α and PI3-K-C2α (Brown et al., 1999), generating signaling intermediates such as Ptd(3,4,5)P_3, Ptd(3)P, and Ptd(3,5)P_2. Interestingly, Ptd(4,5)P_2 and Ptd(3,4,5)P_3 have been reported to stimulate the phosphatase activity of PTP-MEG2 in vitro (Kruger et al., 2002). Thus, the observed regulation of insulin receptor activation and hepatic glucose production by PTP-MEG2 may involve phosphatidylinositol products synthesized in response to insulin receptor signaling. Taken together, these results further define the regulation of insulin signaling in the liver and suggest that pharmacological targeting of PTP-MEG2 may be a potential strategy for the treatment of type 2 diabetes.

Experimental procedures

High-throughput transfection and imaging

High-throughput (retro)transfections of 4800 human and mouse genes from the Mammalian Genome Collection (Strausberg et al., 1999) were carried out as described (Chanda et al., 2003; http://function.gnf.org). In brief, 20 μl mixture of FuGENE 6 (Roche) and GFP-FOXO1 in pcDNA3 (20 ng/well, kindly provided by Professor W.R. Sellers) in DMEM medium (Invitrogen) was added to prespotted 384-well black, clear-bottom plates (Greiner) containing 62.5 ng of plasmid DNA per well. After a 30 min incubation, approximately 2000 U2OS cells (ATCC) in 30 μl of DMEM supplemented with 16% FBS (Invitrogen) and 1.6 mM glutamine (Invitrogen) were added to each well. Cells were grown for 60 hr at 37ºC in 5% CO_2. Cells were washed with PBS in an EMBLA plate washer (Molecular Devices) and fixed with 4% paraformaldehyde in PBS. Nuclei were stained with 4′,6-diamidino-2-phenylindole (200 nM; Molecular Probes) in 0.3% TritonX-100/PBS for 30 min and washed with PBS. Cells were imaged on an IC100 (Beckman) automated inverted fluorescence microscope (Nikon TE300 with a Cohu video camera) with a 10×/0.5 objective (Nikon). Sixteen images were collected per well in two channels using filters appropriate for DAPI and GFP fluorophores. Image analysis was performed with CytoShop software (Beckman). After images were shade-corrected and background-subtracted, objects were extracted and single cells defined using geometric and total fluorescence parameters in the DAPI channel. Transfected cells were identified based on total GFP fluorescence, and the fractional fluorescence in the nucleus (FLIN value) was determined for all GFP-positive cells. FLIN values were averaged for each well, excluding wells with less than eight GFP-positive cells. The number of standard deviations from the mean (σ value) for each gene was calculated as described in the main text. Images in Figure 1 were acquired on a Nikon TE2000 inverted fluorescence microscope using a 40× objective and processed using MetaMorph software (Universal Imaging). Small fluorescent aggregates in the DAPI channel (resulting from DNA precipitates) were removed via image processing for clarity. Percentages of cells with cytoplasmic, mixed, and nuclear GFP-FOXO1 reported in Table S1 were based on counts of >100 fluorescent cells (GFP-FOXO1 fluorescence > 2-fold over background).

Plasmids

hG6Pase (-1227/+57)Luc construct was described previously (Ayala et al., 1999). FOXO1 binding sites at −186 and −172 were disrupted by introduction of point mutations in hG6Pase (−1227/+57) Luc construct as reported (Ayala et al., 1999). To generate the pU6-MEG2 RNAi construct, palindromic sequences corresponding to nucleotides 469–490 from the mouse MEG2 coding sequence (5′-GGGTCTAATTATGCCAACTTTG) were linked to human U6 promoter in the pBluescript KS vector (Strategene). For a negative control, pU6-US construct, an oligonucleotide that does not match with any known gene (5′-GGCATTACAGTATCGATCAGA-3′) was used. The catalytically inactive PTP-MEG2 (C515S) mutant was constructed using the QuikChange site-directed mutagenesis kit following the manufacturer's instructions using the oligos 5′-CACCCATTGTGGTCCATAGCAGTGCAGGCATTG-3′and 5′-CAATGCCTGCACTGCTATGGACCACAATGGGTG-3′. The PTP-MEG2 catalytic subunit fragment was obtained using PCR with the oligos 5′-CCGGAATTCGCCGCCAGCCATGACCATCCAAGAGTTGGTGG-3′ and 5′-ATGCCGCTCGAGTTACTGACTCTCCACGGCCAG-3′ and subcloned into the EcoRI and XhoI sites in pcDNA3 (Invitrogen).

Secreted alkaline phosphatase assay
Secreted alkaline phosphatase (SEAP) assay was performed according to manufacturer's instructions (Great EscAPe reporter system, BD Biosciences). U2OS cells were transfected with a mix of pSEAP-control (BD Biosciences, 10 ng), pGL3 control (Promega, 20 ng) and gene-of-interest (45 ng) per well in a 384-well plate with FuGENE6 as the transfection reagent. 40 hr after transfection, cells were washed with growth medium and treated with Brefeldin A (1.5 μM, Sigma-Aldrich), ethanol, or no stimulus (for PTP-MEG2, PTP-MEG2[C515S], and pcDNA3 transfections) for 4.5 hr. Supernatant was removed and SEAP activity was determined using a chemiluminescent substrate. Background signal (no pSEAP-control transfected) was subtracted from all signals. For normalization, cells were washed with growth medium, and luciferase signal was read using Bright Glo (Promega).

G6Pase reporter transient transfection assays
Human hepatoma HepG2 cells were maintained with Ham's F12 medium supplemented with 10% FBS (Invitrogen). For transfection, Fugene 6 reagent was used according to the manufacturer's instructions. Each transfection was performed with 50 ng of luciferase construct, 25 ng of β galactosidase expression plasmid, and 25 ng each of expression vector for wt PTP-MEG2 or PTP-MEG2 (C515S). If necessary, the empty vector pcDNA3 (Invitrogen) was used to maintain a constant amount of DNA for each transfection. Cells were treated with serum free media +/− 100 nM insulin (Sigma) for 16 hr and were harvested for luciferase assays. The luciferase activity was normalized to β galactosidase activity.

Recombinant adenoviruses
Adenoviruses expressing GFP only or nonspecific RNAi control were described previously (Koo et al., 2004). Adenoviruses for MEG2 or MEG2 RNAi were generated by homologous recombination as described (Koo et al., 2004). The virus contained the cDNA encoding GFP under the control of CMV promoter for monitoring the infection efficiency. For animal experiments, viruses were purified by CsCl method and dialyzed against PBS buffer containing 10% glycerol before the injection.

Culture of primary hepatocytes
Rat primary hepatocytes were prepared from 200–300 g Sprague-Dawley rats by collagenase perfusion method as described previously (Koo et al., 2004). 1×10^6 cells were plated in 6-well plates with medium 199 (Invitrogen) supplemented with 10% FBS, 10 units/ml penicillin, 10 μg/ml streptomycin, and 10 nM dexamethasone for 3–6 hr. After attachment, cells were infected with adenoviruses expressing either GFP alone or GFP and MEG2 for 16 hr. Subsequently, cells were maintained in medium 199 without FBS and dexamethasone for 8 hr and treated with 100 nM insulin for 16 hr.

Quantitative PCR
Total RNA from primary hepatocytes was extracted using RNeasy mini-kit (Qiagen). 500 ng (for primary hepatocytes) of total RNA was used for generating cDNA with Superscript II enzyme (Invitrogen). cDNAs were analyzed by quantitative PCR using SYBR green PCR kit and an ABIPRISM 7700 Sequence detector (Perkin Elmer). All PCR data was normalized to ribosomal L32 expression in the corresponding sample.

Insulin receptor pulldown and anti-phosphotyrosine analysis
HEK-293A cells (Invitrogen) cultured in 10% FBS/DMEM/glutamine were transiently transfected with an empty vector, PTP-MEG2, or PTP-MEG2 (C515) using Effectene transfection reagent (Qiagen). After 2 days, cells were washed with PBS and serum starved in DMEM for 24 hr. Cells were treated with bovine insulin (Sigma) at 10 nM concentration for 30 min. Cells were washed with cold TBS and lysed in 1% triton X-100 in TBS with EDTA (1 mM), protease inhibitors (Roche), sodium fluoride (1 mM) and pervanadate (1 mM), and centrifuged at 20,800 × g. Insulin receptor was immunoprecipitated from the supernatant with anti-insulin receptor β (Upstate Biotechnologies) overnight followed by binding to Protein G resin (Pierce). Resin was washed thoroughly and samples for electrophoresis were prepared by boiling in 3× SDS loading buffer. After SDS-PAGE electrophoresis, proteins were transferred to 0.2 μm nitrocellulose membrane (Schleicher and Schuell) and probed with anti-phosphotyrosine antibody 4G10 (Upstate) or anti-insulin receptor β.

Transient overexpression and immunoblot analysis
HEK-293A cells were transfected with an empty vector control or PTP-MEG2 in 35 mm cell culture dishes. After 48 hr, cells were serum starved for 24 hr and treated with of insulin (20 nM, Sigma) or various concentrations IGF-1 (Sigma). Lysates were prepared as described above, protein concentrations were determined, and equal quantities of protein were loaded in each lane for SDS-PAGE and transfered to nitrocellulose. Blots were probed with anti-InsR phospho-Tyr1162/1163 (EMD Biosciences), anti-InsR β (Santa Cruz), or anti-β-actin (Sigma). The blot shown in Figures 2A and S1A were probed with anti-FOXO1 phospho-Ser256 (Cell Signaling #9461) and anti-FOXO1 (Cell Signaling #9462). For loading control analysis, blots were stripped with 2% SDS in 62.5 mM Tris (pH 6.8) with 100 mM β-mercaptoethanol for 25 min at 56°C and room temperature for 25 min. After washing and blocking, blots were reprobed with antibodies for total protein levels.

Small inhibitor RNA suppression analysis
HepG2 cells were cultured in MEM-α (Cellgro) supplemented with 10% FBS and glutamine at 37°C and 5% CO_2. Cells were plated in 35 mm dishes and transfected with small inhibitor RNA (siRNA) oligos mixed with Lipofectamine 2000 (Invitrogen) following the manufacturer's protocol. siRNA sequences were: MEG2 siRNA 5′-GCAUUUCCAGCUCGUUUGA-3′; mouse Trb3 siRNA 5′-CGAGUGAGAGAUGAGCCUG-3′ (Du et al., 2003); MEG2 smartpool: Dharmacon M-008832-00. After 48 hr, cells were washed with PBS and serum starved in MEM-α/glutamine for 24 hr. Cells were treated with insulin (3 nM) for 30 min and lysed as described above. Lysates were analyzed by Western blot as described above. PTP-MEG2 levels were probed with a rabbit polyclonal antibody 1489B raised against the peptide sequence RPDMAPELTPEEE conjugated to keyhole limpet hemocyanin (Imgenex). Akt phosphorylation was examined using anti-Akt (phospho-S473) and anti-Akt (Cell Signaling #9271 and #9272, respectively).

Short hairpin RNA-mediated reduction of PTP-MEG2 expression
PTP-MEG2 RNAi adenovirus and a control RNAi adenovirus were used to infect glucose-6-phosphatase promoter-luciferase stable H4IIE cells (kind gift from N. Gekakis) in 10% FBS/DMEM with glutamine. After 48 hr, cells were serum starved in DMEM with glutamine for 24 hr. Cells were treated with 25 μM dexamethasone (Sigma) and various concentrations of insulin for 24 hr. Luciferase signals were read by the addition of BrightGlo reagent (Promega) and read on an Analyst plate reader (Molecular Devices).

Animal experiments
Male 7-week-old C57BL6 mice or db/db mice were purchased from Harlan or Jackson Laboratory and maintained in regular chow under the 12 hr light-dark cycle. 0.5×10^9 plaque-forming units per recombinant adenovirus were delivered by a systemic tail vain injection to mice that were anaesthetized with Iso-Flurane. For measuring fasting blood glucose level, animals were fasted for 16 hr or 5 hr with free access to water. Blood glucose was monitored at the end of each fasting period for designated time points listed in the figure legends. Liver tissues were collected at the end of experiments and immediately frozen in liquid nitrogen. Western blot analysis was performed with GFP antibody to check the relative infection.

Glucose tolerance test
5–7 days post injections, mice were fasted for 16 hr (WT) or 5 hr (*db*/*db* mice) prior to the glucose tolerance test. Mice were injected intraperitoneally with 2 g/kg body weight of glucose. Blood glucose levels were measured from tail vein blood collected at the designated time periods listed in the figure legends using an automated glucose monitor (One Touch, Lifescan).

Insulin tolerance test
4–5 days post injections, 5 hr-fasted (WT) or ad lib fed (*db*/*db* mice) mice were injected intraperitoneally with 1 unit/kg body weight of insulin. Blood glucose levels were measured from tail vein blood collected at the designated time periods listed in the figure legends.

Fasting and refeeding experiments
Wild-type C57/Bl6 adult male mice (6 per group) were fed ad libitum, fasted for 16 hr, or fasted for 24 hr and refed for 24 hr. Total RNA was extracted from liver samples in Trizol (Invitrogen) using the RNeasy kit with DNase treatment. cDNA was generated using the high capacity cDNA archive kit (Applied

Biosystems). Real-time polymerase chain reaction (PCR) was performed using Taqman probes labeled with carboxyfluorescein (FAM) dye for the relevant genes (PTPN9: probe Mm00451036_m1; PEPCK: probe Mm00440636_m1 from Applied Biosystems) with a probe for mouse ribosomal protein 36B4 (VIC labeled) as an internal standard. Real time PCR was monitored on a Sequence Detection System 7900HT (Applied Biosystems); reactions were run in triplicate.

Supplemental data

Supplemental data include five figures and two tables and can be found with this article online at http://www.cellmetabolism.org/cgi/content/full/3/5/367/DC1/.

Acknowledgments

The authors would like to thank Dr. Nathanael Gray and Prof. William Sellers for helpful discussions, Dr. Shihmin Huang and Dr. Nicholas Gekakis for cell lines and discussion, and Abel Gutierrez, Paul DeJesus, Myleen Medina, Suhaila White, Brendan Smith, and Sandy Bohan for technical support. This work was supported by the Novartis Research Foundation. This paper is dedicated to the memory of Dr. Thomas Byung-Mo Cho.

Received: July 18, 2005
Revised: December 1, 2005
Accepted: March 9, 2006
Published: May 9, 2006

References

Accili, D., and Arden, K. (2004). FoxOs at the crossroads of cellular metabolism, differentiation, and transformation. Cell *117*, 421–426.

Alonso, A., Sasin, J., Bottini, N., Friedberg, I., Friedberg, I., Osterman, A., Godzik, A., Hunter, T., Dixon, J., and Mustelin, T. (2004). Protein tyrosine phosphatases in the human genome. Cell *117*, 699–711.

Altomonte, J., Richter, A., Harbaran, S., Suriawinata, J., Nakae, J., Thung, S.N., Meseck, M., Accili, D., and Dong, H. (2003). Inhibition of Foxo1 function is associated with improved fasting glycemia in diabetic mice. Am. J. Physiol. Endocrinol. Metab. *285*, E718–E728.

Altomonte, J., Cong, L., Harbaran, S., Richter, A., Xu, J., Meseck, M., and Dong, H.H. (2004). Foxo1 mediates insulin action on apoC-III and triglyceride metabolism. J. Clin. Invest. *114*, 1493–1503.

Asante-Appiah, E., and Kennedy, B.P. (2003). Protein tyrosine phosphatases: the quest for negative regulators of insulin action. Am. J. Physiol. Endocrinol. Metab. *284*, E663–E670.

Ayala, J.E., Streeper, R.S., Desgrosellier, J.S., Durham, S.K., Suwanichkul, A., Svitek, C.A., Goldman, J.K., Barr, F.G., Powell, D.R., and O'Brien, R.M. (1999). Conservation of an insulin response unit between mouse and human glucose-6-phosphatase catalytic subunit gene promoters: transcription factor FKHR binds the insulin response sequence. Diabetes *48*, 1885–1889.

Barthel, A., and Schmoll, D. (2003). Novel concepts in insulin regulation of hepatic gluconeogenesis. Am. J. Physiol. Endocrinol. Metab. *285*, E685–E692.

Barthel, A., Schmoll, D., and Unterman, T.G. (2005). FoxO proteins in insulin action and metabolism. Trends Endocrinol. Metab. *16*, 183–189.

Brown, R.A., Domin, J., Arcaro, A., Waterfield, M.D., and Shepherd, P.R. (1999). Insulin activates the alpha isoform of class II phosphoinositide 3 kinase. J. Biol. Chem. *274*, 14529–14532.

Brunet, A., Bonni, A., Zigmond, M.J., Lin, M.Z., Juo, P., Hu, L.S., Anderson, M.J., Arden, K.C., Blenis, J., and Greenberg, M.E. (1999). Akt promotes cell survival by phosphorylating and inhibiting a Forkhead transcription factor. Cell *96*, 857–868.

Brunet, A., Park, J., Tran, H., Hu, L.S., Hemmings, B.A., and Greenberg, M.E. (2001). Protein kinase SGK mediates survival signals by phosphorylating the forkhead transcription factor FKHRL1 (FOXO3a). Mol. Cell. Biol. *21*, 952–965.

Brunet, A., Sweeney, L.B., Sturgill, J.F., Chua, K.F., Greer, P.L., Lin, Y., Tran, H., Ross, S.E., Mostoslavsky, R., Cohen, H.Y., et al. (2004). Stress-dependent regulation of FOXO transcription factors by the SIRT1 deacetylase. Science *303*, 2011–2015.

Chanda, S.K., White, S., Orth, A.P., Reisdorph, R., Miraglia, L., Thomas, R.S., DeJesus, P., Mason, D.E., Huang, Q., Vega, R., et al. (2003). Genome-scale functional profiling of the mammalian AP–1 signaling pathway. Proc. Natl. Acad. Sci. USA *100*, 12153–12158.

Cho, H., Mu, J., Kim, J.K., Thorvaldsen, J.L., Chu, Q., Crenshaw, E.B., 3rd, Kaestner, K.H., Bartolomei, M.S., Shulman, G.I., and Birnbaum, M.J. (2001). Insulin resistance and a diabetes mellitus-like syndrome in mice lacking the protein kinase Akt2 (PKB beta). Science *292*, 1728–1731.

Du, K., Herzig, S., Kulkarni, R.N., and Montminy, M. (2003). TRB3: a tribbles homolog that inhibits Akt/PKB activation by insulin in liver. Science *300*, 1574–1577.

Elchebly, M., Payette, P., Michaliszyn, E., Cromlish, W., Collins, S., Loy, A.L., Normandin, D., Cheng, A., Himms-Hagen, J., Chan, C.C., et al. (1999). Increased insulin sensitivity and obesity resistance in mice lacking the protein tyrosine phosphatase-1B gene. Science *283*, 1544–1548.

Ellis, L., Clauser, E., Morgan, D.O., Edery, M., Roth, R.A., and Rutter, W.J. (1986). Replacement of insulin receptor tyrosine residues 1162 and 1163 compromises insulin-stimulated kinase activity and uptake of 2-deoxyglucose. Cell *45*, 721–732.

Galic, S., Klingler-Hoffmann, M., Fodero-Tavoletti, M.T., Puryer, M.A., Meng, T.C., Tonks, N.K., and Tiganis, T. (2003). Regulation of insulin receptor signaling by the protein tyrosine phosphatase TCPTP. Mol. Cell. Biol. *23*, 2096–2108.

Galic, S., Hauser, C., Kahn, B.B., Haj, F.G., Neel, B.G., Tonks, N.K., and Tiganis, T. (2005). Coordinated regulation of insulin signaling by the protein tyrosine phosphatases PTP1B and TCPTP. Mol. Cell. Biol. *25*, 819–829.

Haj, F.G., Verveer, P.J., Squire, A., Neel, B.G., and Bastiaens, P.I. (2002). Imaging sites of receptor dephosphorylation by PTP1B on the surface of the endoplasmic reticulum. Science *295*, 1708–1711.

Harada, J.N., Bower, K.E., Orth, A.P., Callaway, S., Nelson, C.G., Laris, C., Hogenesch, J.B., Vogt, P.K., and Chanda, S.K. (2005). Identification of novel mammalian growth regulatory factors by genome scale quantitative image analysis. Genome Res. *15*, 1136–1144.

Huynh, H., Wang, X., Li, W., Bottini, N., Williams, S., Nika, K., Ishihara, H., Godzik, A., and Mustelin, T. (2003). Homotypic secretory vesicle fusion induced by the protein tyrosine phosphatase MEG2 depends on polyphosphoinositides in T cells. J. Immunol. *171*, 6661–6671.

Huynh, H., Bottini, N., Williams, S., Cherepanov, V., Musumeci, L., Saito, K., Bruckner, S., Vachon, E., Wang, X., Kruger, J., et al. (2004). Control of vesicle fusion by a tyrosine phosphatase. Nat. Cell Biol. *6*, 831–839.

Klaman, L.D., Boss, O., Peroni, O.D., Kim, J.K., Martino, J.L., Zabolotny, J.M., Moghal, N., Lubkin, M., Kim, Y.B., Sharpe, A.H., et al. (2000). Increased energy expenditure, decreased adiposity, and tissue-specific insulin sensitivity in protein-tyrosine phosphatase 1B-deficient mice. Mol. Cell. Biol. *20*, 5479–5489.

Koo, S.H., Satoh, H., Herzig, S., Lee, C.H., Hedrick, S., Kulkarni, R., Evans, R.M., Olefsky, J., and Montminy, M. (2004). PGC-1 promotes insulin resistance in liver through PPAR-alpha-dependent induction of TRB-3. Nat. Med. *10*, 530–534.

Kruger, J.M., Fukushima, T., Cherepanov, V., Borregaard, N., Loeve, C., Shek, C., Sharma, K., Tanswell, A.K., Chow, C.W., and Downey, G.P. (2002). Protein-tyrosine phosphatase MEG2 is expressed by human neutrophils. Localization to the phagosome and activation by polyphosphoinositides. J. Biol. Chem. *277*, 2620–2628.

Motta, M.C., Divecha, N., Lemieux, M., Kamel, C., Chen, D., Gu, W., Bultsma, Y., McBurney, M., and Guarente, L. (2004). Mammalian SIRT1 represses forkhead transcription factors. Cell *116*, 551–563.

Nakae, J., Biggs, W.H., 3rd, Kitamura, T., Cavenee, W.K., Wright, C.V., Arden, K.C., and Accili, D. (2002). Regulation of insulin action and pancreatic

beta-cell function by mutated alleles of the gene encoding forkhead transcription factor Foxo1. Nat. Genet. *32*, 245–253.

Nakamura, N., Ramaswamy, S., Vazquez, F., Signoretti, S., Loda, M., and Sellers, W.R. (2000). Forkhead transcription factors are critical effectors of cell death and cell cycle arrest downstream of PTEN. Mol. Cell. Biol. *20*, 8969–8982.

Puigserver, P., Rhee, J., Donovan, J., Walkey, C.J., Yoon, J.C., Oriente, F., Kitamura, Y., Altomonte, J., Dong, H., Accili, D., and Spiegelman, B.M. (2003). Insulin-regulated hepatic gluconeogenesis through FOXO1-PGC-1alpha interaction. Nature *423*, 550–555.

Ren, J.M., Li, P.M., Zhang, W.R., Sweet, L.J., Cline, G., Shulman, G.I., Livingston, J.N., and Goldstein, B.J. (1998). Transgenic mice deficient in the LAR protein-tyrosine phosphatase exhibit profound defects in glucose homeostasis. Diabetes *47*, 493–497.

Salomon, A.R., Ficarro, S.B., Brill, L.M., Brinker, A., Phung, Q.T., Ericson, C., Sauer, K., Brock, A., Horn, D.M., Schultz, P.G., and Peters, E.C. (2003). Profiling of tyrosine phosphorylation pathways in human cells using mass spectrometry. Proc. Natl. Acad. Sci. USA *100*, 443–448.

Strausberg, R.L., Feingold, E.A., Klausner, R.D., and Collins, F.S. (1999). The mammalian gene collection. Science *286*, 455–457.

Su, A.I., Wiltshire, T., Batalov, S., Lapp, H., Ching, K.A., Block, D., Zhang, J., Soden, R., Hayakawa, M., Kreiman, G., Cooke, M.P., Walker, J.R., and Hogenesch, J.B. (2004). A gene atlas of the mouse and human protein-encoding transcriptomes. Proc. Natl. Acad. Sci. USA *101*, 6062–6067.

Ueki, K., Yballe, C.M., Brachmann, S.M., Vicent, D., Watt, J.M., Kahn, C.R., and Cantley, L.C. (2002). Increased insulin sensitivity in mice lacking p85beta subunit of phosphoinositide 3-kinase. Proc. Natl. Acad. Sci. USA *99*, 419–424.

Wang, X., Huynh, H., Gjorloff-Wingren, A., Monosov, E., Stridsberg, M., Fukuda, M., and Mustelin, T. (2002). Enlargement of secretory vesicles by protein tyrosine phosphatase PTP-MEG2 in rat basophilic leukemia mast cells and Jurkat T cells. J. Immunol. *168*, 4612–4619.

Wang, Y., Vachon, E., Zhang, J., Cherepanov, V., Kruger, J., Li, J., Saito, K., Shannon, P., Bottini, N., Huynh, H., et al. (2005). Tyrosine phosphatase MEG2 modulates murine development and platelet and lymphocyte activation through secretory vesicle function. J. Exp. Med. *202*, 1587–1597.

White, M.F. (2003). Insulin signaling in health and disease. Science *302*, 1710–1711.

Zabolotny, J.M., Kim, Y.B., Peroni, O.D., Kim, J.K., Pani, M.A., Boss, O., Klaman, L.D., Kamatkar, S., Shulman, G.I., Kahn, B.B., and Neel, B.G. (2001). Overexpression of the LAR (leukocyte antigen-related) protein-tyrosine phosphatase in muscle causes insulin resistance. Proc. Natl. Acad. Sci. USA *98*, 5187–5192.

Zhao, R., Fu, X., Li, Q., Krantz, S.B., and Zhao, Z.J. (2003). Specific interaction of protein tyrosine phosphatase-MEG2 with phosphatidylserine. J. Biol. Chem. *278*, 22609–22614.